World Scientific
www.worldscientific.com

Separation of cortical arteries and veins in optical neurovascular imaging

Linna Zhao[*,‡], Yao Li[*,†,§,**], Hongyang Lu[*,†], Lu Yuan[*,†]
and Shanbao Tong[*,†,¶,**]

[*]Med-X Research Institute, Shanghai Jiao Tong University
1954 Huashan Rd., Shanghai 200030, P. R. China

[†]School of Biomedical Engineering
Shanghai Jiao Tong University
800 Dongchuan Rd., Shanghai 200240, P. R. China

[‡]School of Life Science and Technology
Huazhong University of Science and Technology
1037 Luoyu Rd., Wuhan 430074, P. R. China
[§]yaoli118@gmail.com
[¶]shanbao.tong@gmail.com

Separation of arteries and veins in the cerebral cortex is of significant importance in the studies of cortical hemodynamics, such as the changes of cerebral blood flow, perfusion or oxygen concentration in arteries and veins under different pathological and physiological conditions. Yet the cerebral vessel segmentation and vessel-type separation are challenging due to the complexity of cortical vessel characteristics and low spatial signal-to-noise ratio. In this work, we presented an effective full-field method to differentiate arteries and veins in cerebral cortex using dual-modal optical imaging technology including laser speckle imaging (LSI) and optical intrinsic signals (OIS) imaging. The raw contrast images were acquired by LSI and processed with enhanced laser speckle contrast analysis (eLASCA) algorithm. The vascular pattern was extracted and segmented using region growing algorithm from the eLASCA-based LSI. Meanwhile, OIS images were acquired alternatively with 630 and 870 nm to obtain an oxyhemoglobin concentration map over cerebral cortex. Then the separation of arteries and veins was accomplished by Otsu threshold segmentation algorithm based on the OIS information and segmentation of LSI. Finally, the segmentation and separation performances were assessed using area overlap measure (AOM). The segmentation and separation of cerebral vessels in cortical optical imaging have

[**]Corresponding authors.

great potential applications in full-field cerebral hemodynamics monitoring and pathological study of cerebral vascular diseases, as well as in clinical intraoperative monitoring.

Keywords: Vessel segmentation; laser speckle imaging; optical intrinsic signals imaging; region growing algorithm; artery–vein separation.

1. Introduction

Cortical vessel separation is highly valuable in cerebral hemodynamics study, and plays an important role in clinical diagnostic and therapeutic management of a variety of vascular diseases, e.g., cerebral hemorrhage, stroke, aneurysm, etc.[1] Therefore, an effective method is in great need to separate arteries and veins from cerebral cortical vessels.

The separation of arteries and veins has been investigated using different methods for vessel-type identification, mostly in the separation of retinal vessels. Li *et al.* proposed a piecewise Gaussian model for retinal vessels utilizing the central reflex characteristics to describe the image intensity distribution.[2] Narasimha-Iyer *et al.* developed an automated methodology to identify arteries and veins from dual-wavelength retinal fundus images recorded at 570 and 600 nm utilizing both structural and functional features of the images.[3] Mendonca and Campilho proposed a set of four directional differential operators for detecting the vessel centerlines and then applied a binary morphological reconstruction method and a region growing process to segment the vessels.[4]

However, there has been few literature reviews on the identification of cortical vessel types based on the differences between arteries and veins in different aspects. For example, Wang *et al.* presented a method for separating cortical arteries and veins in optical intrinsic signals (OIS) using 0.1-Hz oscillation at the wavelengths of 546 and 630 nm. Multiscale matched filter and a single Gaussian model were employed to acquire different vessel types.[5] Zhong *et al.* applied a method of independent component analysis (ICA) to OIS images and separated the arterial and venous regions. They constructed a feature vector combining heartbeat and respiration features for the fuzzy c-means clustering method and determined the vessel types using morphological intersection points.[6] Hu *et al.* identified the vessel-type based on the phenomenon that the spectral distribution of OIS was different between arterial and venous vessels.[7] Vanzetta *et al.* identified different cortical microvascular compartments in anesthetized cats by the ratio image of two wavelengths at 540 and 560 nm, which were corresponding to the peaks of oxyhemoglobin (HbO) and deoxyhemoglobin (HbR), respectively. Yet the absorption coefficients differences at these two wavelengths for HbR and HbO are not high enough for artery–vein separation in low signal-to-noise ratio images, e.g., rodent cerebral cortical vessels.[8] Nevertheless, due to the low signal-to-noise ratio, these OIS-based vessel-type separation methods have a fair performance in spatial resolution.

Compared with other imaging techniques, laser speckle imaging (LSI) provides a two-dimensional real-time, full-field cerebral blood flow (CBF) velocity map with high spatiotemporal resolution.[9] The CBF velocity information was acquired by laser speckle contrast analysis (LASCA). While OIS imaging is a useful tool for functional brain imaging, it can obtain oxygen distribution information in vessels and tissues.[10] The differences in the concentration of oxygen–hemoglobin between arteries and veins could be used to differentiate arteries and veins.

In this paper, we proposed a separation method using dual-modal optical imaging techniques, i.e., LSI and OIS, to achieve a high spatial resolution for vessel-type separation. We extracted the vessel pattern based on LSI using region growing algorithm. Then OIS images were acquired at the wavelengths of 630 nm and 870 nm, so that we might distinguish the concentration of HbO in arteries and veins by computing the differences of reflected light intensity at 630 nm and at 870 nm. Finally, arteries and veins would be separated by Otsu thresholding algorithm. Besides, we used area overlap measure (AOM) to evaluate the segmentation and separation performance.

2. Materials and Methods

2.1. *Animal preparation*

The experimental protocols in this study were approved by the Animal Care and Use Committee

of Med-X Research Institute of Shanghai Jiao Tong University. One male adult Sprague-Dawaley (SD) (240 g) rat was used in the experiment. Firstly, the rat was anesthetized with chloral hydrate (350 mg/kg, IP, 7%) and then mounted to a stereotaxic frame (Benchmark DeluxeTM, MyNeurolab.com, St. Louis, MO). During the experiment, the body temperature of the animal was maintained at $37 \pm 0.2°C$ using a DC control module (FHC Inc., Bowdoinham, ME, USA) and a heating pad. After removing the rat hair and epidermal tissue, the skull between bregma and lambda was polished using a dental drill (Fine Science Tools Inc., North Vancouver, Canada) and sterilized with saline until the cerebral vessels were clearly visible.

2.2. *Data collection*

The raw images were captured through the dual-modal optical imaging system (see Fig. 1), which consisted of a CCD camera (12 bit, 24 fps, exposure time, 5 ms), one lens with a focal length of 8 mm (C240TM, Thorlabs), two light emitting diodes (LED630E, Thorlabs and LED870E, Thorlabs) powered by two driver modules (LEDD1B, Thorlabs), a laser diode (L780P010, Thorlabs) powered by a driver module (LDC220C, Thorlabs) and a computer for acquiring image data.

The cortical vessel network was focused and clearly seen by finely tuning the lens. Then the raw speckle images and OIS images at two wavelengths were alternatively captured at a sampling frequency of 24 fps for 200 frames.

2.3. *Principles of LSI and OIS*

LSI is a real-time, full-field and high-resolution CBF imaging technology, utilizing the scattering property of the moving particles to coherent light to obtain a two-dimensional CBF velocity distribution map.[11] Speckle pattern can be described using statistics since it is a random interference pattern.

According to the principle of LSI,[12] speckle contrast K and the CBF velocity obeyed the following relations

$$K = \beta^{0.5} \left\{ \frac{\tau_c}{T} + \frac{\tau_c^2}{2T^2} \left[\exp\left(-\frac{2T}{\tau_c}\right) - 1 \right] \right\}^{0.5}, \quad (1)$$

where β represents the loss of correlation determined by the ratio of the detector size to the speckle size and polarization characteristics of scattered light, τ_c denotes the correlation time, T is the exposure time of CCD. Bonner and Nossal[13] demonstrated that the correlation time

$$\tau_c = 1/ak_0 v, \quad (2)$$

where K_0 is the light wavenumber, a is determined by the particle Lorentzian width and scattering properties, and v is the particle velocity. When K^2 is limited to very small values, e.g., [0, 0.1],[14] it could be induced from Eqs. (1) and (2) that

$$v \propto \frac{1}{K^2}. \quad (3)$$

Equation (3) indicates that CBF velocity is inversely proportional to the square of speckle contrast. Therefore it is obvious that the smaller the contrast, the greater the CBF velocity in the two-dimensional LSI.
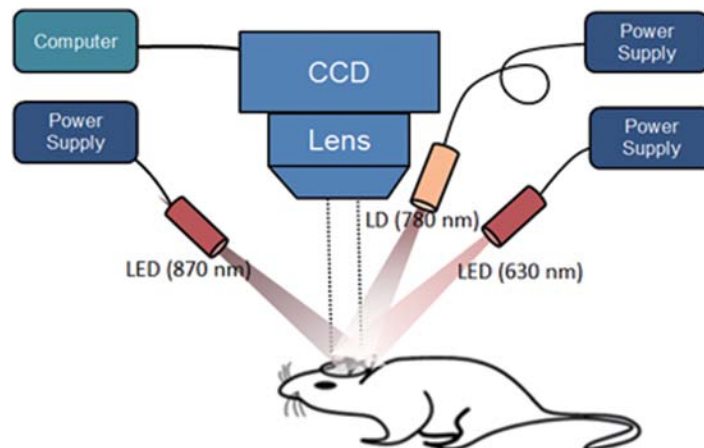

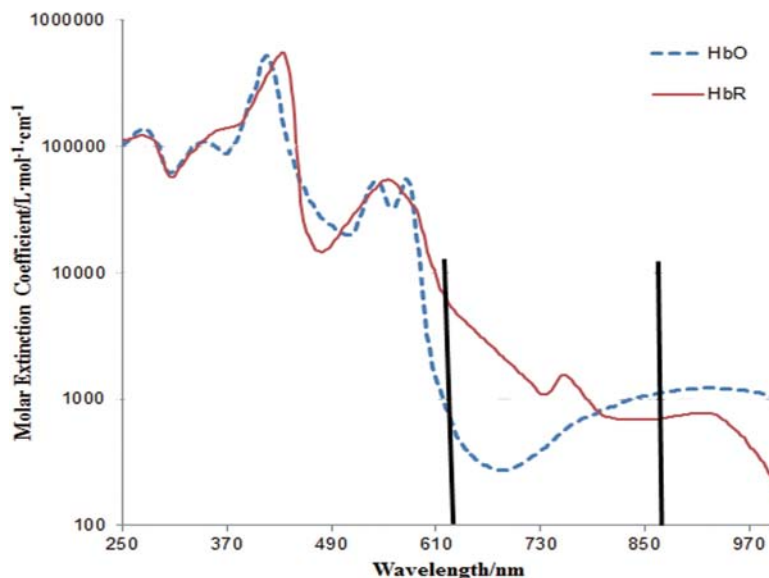Fig. 1.   Illustration of dual-modal optical imaging.

Fig. 2. The molar absorption coefficient. Data is from the website: http://omlc.ogi.edu/spectra/hemoglobin/.

Changes in neuronal activity in the cerebral cortex are coupled to changes in the blood flow and oxygenation, which provide signals that can be measured by OIS imaging.[15] These intrinsic signals measured are now considered to primarily originate from variations in the concentrations of oxyhemoglobin ([HbO]) and deoxyhemoglobin ([HbR]).[16] Although the spatial distribution of functional activations can be qualitatively mapped with single-wavelength OIS, no quantitative information about concentration of total hemoglobin ([HbT]), oxygenation or blood flow could be obtained. To quantify relative [HbO] and [HbR], we used a method of multiple wavelengths.[17]

It is evident in Fig. 2[18] that the absorption coefficient variation of HbR is much larger than that of HbO due to the fact that the absorption of HbR is more sensitive to wavelength than HbO within the range from 550 to 900 nm, which can be used to detect the [HbO]/[HbR].

2.4. Data preprocessing

Firstly, laser speckle contrast images were obtained by random process estimator (RPE) approach after noise reduction and registration.[14] As shown in Fig. 3, the vascular network had a low gray contrast and was interfered by various noises due to
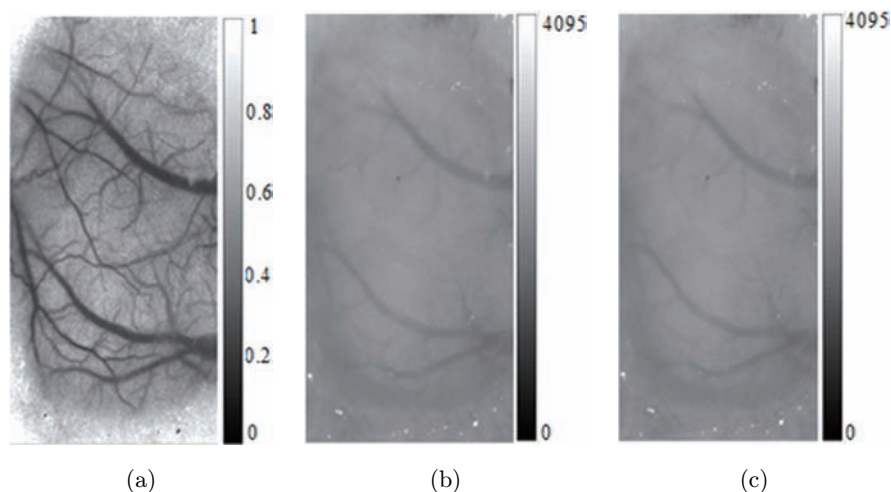

Fig. 3. LSI and OIS images (a) LSI image (b) OIS image at 630 nm (c) OIS image at 870 nm.

respiration, heartbeat and 0.1-Hz low-frequency vessel motion.[19] Hence noise reduction and image enhancement were essential to achieve good vessel segmentation performance.

(1) *Noise Reduction*
Noise reduction was accomplished by a linear anisotropic Gaussian filtering algorithm[20] within a sliding window (3×3) along orientations of $0°$, $45°$, $90°$, $135°$, $180°$, $225°$, $270°$, $315°$, respectively. Because $0°$ and $180°$, $45°$ and $225°$, $90°$ and $270°$, $135°$ and $315°$ are in the same lines respectively, we only investigated gray-intensity differences along the orientations of $0°$, $45°$, $90°$ and $135°$ regardless of the actual vessel directions. Mean square error (MSE) along each orientation was used to determine the vessel direction

$$\text{MSE} = \sqrt{\frac{1}{N} \sum_{i=1}^{N} (x_i - \mu)^2}, \qquad (4)$$

where x_i represents the ith pixel gray level, N represents the pixels number and μ represents the mean gray level in each direction. The orientation with minimal MSE would be considered as the vessel direction. Then we implemented convolution adaptive filter with Gaussian kernel to process laser speckle contrast images.[21]

$$I(x,y) = \int_\infty^\infty \int_\infty^\infty I(x',y')G(x - x', y \\ - y')dx'dy', \qquad (5)$$

where $I(x',y')$ denotes the input image, G is the Gaussian kernel and $I(x,y)$ presents the output image.

(2) *Image Enhancement*
The laser speckle contrast images were enhanced by utilizing enhanced laser speckle contrast analysis (eLASCA) algorithm based upon monotonic point transformation (MPT), which not only improved the CBF visualization but also reserved the CBF variability. Technical details have been reported in Ref. 22.

The three-dimensional K^2 was reshaped into one-dimensional variable $f(i)$ $(i = 1, 2 \ldots M \times N \times L)$ by the following equation[22]:

$$k^2(m,n,l) = f(m + (n - 1) \times M + (l - 1) \\ \times M \times N), \qquad (6)$$

where $M \times N$ is the spatial size of an image, L represents the number of total frames and $m \in$ $[1, M]$; $n \in [1, N]$; $l \in [1, L]$. Then Eq. (7) transformed f into f_e within a much broader range from 0 to 1. In practice, f_e could be approximately computed as[22]

$$f_e = \frac{\text{Num}_f}{M \times N \times L} \times 100\%, \qquad (7)$$

where Num_f denotes the number of pixels with contrast values not more than f.

Finally, the enhanced laser speckle contrast images were obtained by mapping f_e back to three-dimensional K^2 according to Eq. (6).

2.5. *Vessel segmentation*

Cortical vessel segmentation was based on seeded region growing (SRG) algorithm in the following steps.

(1) *Selecting Seed Points*
The growing points, i.e., seed points, were manually selected by visual inspection of the images as human eyes were the gold standard to distinguish the pixels representing the vessel network. To speed up the segmentation, each image was divided into top and bottom halves so that both parts could use SRG simultaneously with three seed points in each.

(2) *The Homogeneity Criterion*
The pixels were merged into the growing region based on an appropriate homogeneity criterion, e.g., gray level value, region connectivity or statistical parameters.[23] In this work, the homogeneity criterion was based on the vessel gray level value, and $\delta(x,y)$ was defined as the difference between merged region and its adjacent pixels,[24]

$$\delta(x,y) = |I(x,y) - \text{mean}_{(x',y')\in A}\{I(x',y')\}|, \quad (8)$$

where A is the merged region, $I(x',y')$ is the gray level of the pixel in A, $I(x,y)$ is the gray level of the adjacent point around A. The gray level value at the lowest trough of the image gray histogram was selected as the initial threshold. If $\delta(x,y)$ is less than the threshold, this pixel would be merged into the growing region, otherwise the pixel would not be merged. The optimal threshold was determined by estimating the degree of region overlap, i.e., AOM described in next section, between the segmented images based on algorithm and the manually segmented images. When the degree of region overlap reached the maximum, we regarded the corresponding threshold as the optimal threshold. The above process was repeated until all the pixels were tested.

(3) *The Assessment of Segmentation*
It was necessary to quantitatively analyze the segmentation performance by comparing the result based on SRG with that by manual segmentation. We used AOM as the criterion for similarity measurement,[25]

$$\text{AOM}(A, B) = \frac{\text{area}\{S_A \cap S_B\}}{\text{area}\{S_A \cup S_B\}}, \qquad (9)$$

where S_A represents the segmentation region with SRG and S_B represents the manual segmentation region. The manual segmentation was based on hand-sketching by a person with neurovascular observation knowledge. $\text{AOM}(A, B) = 1$ indicates that S_A and S_B are completely matching, while AOM $(A, B) = 0$ means that S_A and S_B have no overlap.

2.6. *The separation of arteries and veins*

After the segmentation of vessels, we focused on the pixels of segmented cortical vessels by multiplying the OIS image with the well-segmented vessel binary image.

(1) *The Ratio of Dual-Wavelength OIS Images*
In Fig. 2, we noticed that the absorption coefficient of HbR was obviously higher than that of HbO at 630 nm, implying that this wavelength was sensitive to the concentration change of HbR. And the absorption coefficient of HbR at 870 nm was much lower than that of HbO, indicating that 870-nm light was sensitive to the concentration change of HbO.[3,26]

Therefore, we defined the ratio R of gray level intensity at 630 nm to that at 870 nm:

$$R = \frac{G_{630}}{G_{870}}, \qquad (10)$$

where G_{630} and G_{870} represent the intensities of reflected light at 630 and 870 nm, respectively. By applying dual-wavelength OIS imaging, we could get the distribution of relative [HbO] and [HbR] in cortical vessels for further artery–vein separation.

(2) *Automatic Segmentation by Otsu Thresholding*
We accomplished the separation of arteries and veins using the ratio R of dual-wavelength OIS images by Otsu automatic thresholding algorithm.[27]

Firstly, the image was divided equally into two parts in order to determine the threshold more accurately. If each OIS image (R) has N pixels with

L gray level, the probability p_i of each gray level could be denoted as

$$p_i = \frac{f(i)}{N} \quad (i = 1, 2, \ldots, L), \qquad (11)$$

where $f(i)$ represents the number of pixels at ith gray level. An initial threshold t $(1 < t < L)$ was used to divide the gray levels into two groups C_1 and C_2, where C_1 contained the gray levels from 1 to t and C_2 contained the gray levels from $t + 1$ to L.

The between-class variance σ^2 was defined to determine the optimal threshold t':

$$\sigma^2 = w_1(u_1 - u)^2 + w_2(u_2 - u)^2, \qquad (12)$$

where w_1 and w_2 represent total probabilities of class C_1 and class C_2, respectively, and u is the mean of the whole gray levels. The threshold t' corresponded to t when σ^2 reached the maximum value.

After the separation, AOM would be used to assess the separation performance.

3. Results

3.1. *Vessel segmentation using LSI*

Figure 4(c) is the segmented cortical vessel network. It is shown that major vessels were well segmented while some of the small vessels were missed. This is due to the fact that region growing algorithm is based on gray levels of the image. But from Fig. 4(a), we could hardly differentiate the small vessels from capillary bed. In our work, we selected an appropriate threshold for segmenting the major vessels.

According to Eq. (9), AOM between SRG-based separation [see Fig. 4(c)] and manual separation [see Fig. 4(b)] reached 76.59% (see Table 1), which indicated that we achieved a good segmentation performance.

3.2. *The separation of arteries and veins*

Figures 5(a) and 5(b) show the OIS vessel network at 630 nm and 870 nm, respectively. We noticed that it was very difficult to distinguish arteries and veins by a single-wavelength OIS image. The ratio R of OIS Images is shown in Fig. 5(c), in which the gray intensities in veins are obviously lower than those of arteries. Figure 5(d) illustrates the cortical vessel artery–vein separation using our proposed method, in which the blue vessels represent veins
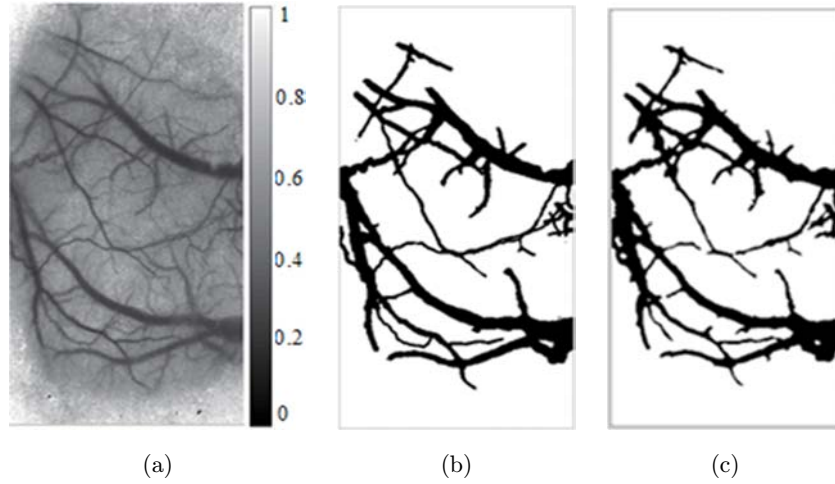
Fig. 4.   Vessel segmentation (a) LSI (b) the manual segmentation (c) the segmentation with SRG.
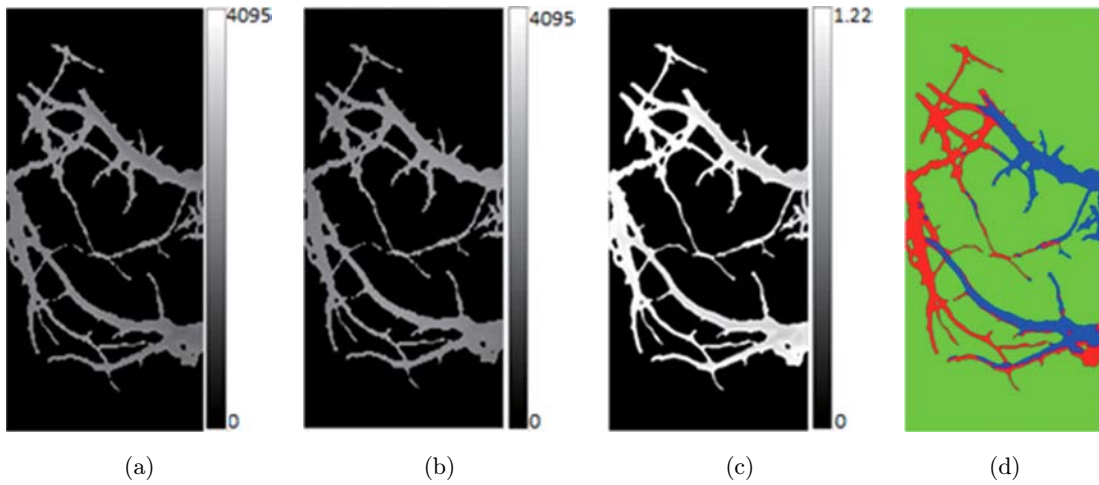

Fig. 5.   The separation of arteries and veins (a) OIS vessel network at 630 nm (b) OIS vessel network at 870 nm (c) The ratio R of OIS images (d) The artery–vein separation (the blue vessels represent veins and the red vessels represent arteries).

Fig. 6.   Arteries and veins (a) arteries criterion (b) the segmentation of arteries (c) vein criterion (d) the segmentation of veins.

Table 1. AOM of different vessel types.

Vessel type	Vessels	Arteries	Veins
AOM	76.59%	57.39%	64.99%

Note: AOM: area overlap measure.

and the red vessels represent arteries. It was found that the major arteries and veins over the major somatosensory area were correctly separated although there were a few errors in the overlapping regions. Due to the influence of CCD depth of field, pia mater arteries and capillaries were also mistakenly classified into cortical vessels. Also, a small number of veins near the window edge were wrongly segmented as arteries due to higher noise level around the window edge area.

In Fig. 6, the arteries and veins criteria were also separated by experts according to their experiences. The overlaps of the arteries and veins were computed by Eq. (9) and the AOMs of them were 57.39% and 64.99% (see Table 1), respectively. As shown in Fig. 6(b), the segmentation of arteries was not performed optimally, among which a small part of veins were wrongly classified into arteries. By comparing Figs. 6(c) with 6(d), we found the major veins were well separated out except the edge area with low signal-to-noise ratio.

4. Discussion and Conclusions

In this work, we proposed an effective and efficient method for cortical artery–vein separation combining LSI with OIS imaging. Compared with other vessel-type classification methods, this method took advantage of full-field high spatiotemporal resolution LSI to segment cortical vessel network, thus achieving better performance than only OIS-based segmentation. Yet one limitation is that the SRG is a semi-automated segmentation because the seeds were selected manually. Another limitation was that the small vessels were not well segmented due to low signal-to-noise ratio between small vessels and the capillary bed while the segmentation of major vessels worked well. The classification of veins was better than arteries especially in vessel overlapping area. Because major vessels should be paid more attention during neurosurgery, our method provides a convenient and efficient way to the artery–vein separation with potential clinical and research applications.

References

1. J. F. Sabik, B. W. Lytle, P. M. McCarthy, D. M. Cosgrove, "Axillary artery: An alternative site of arterial cannulation for patients with extensive aortic and peripheral vascular disease," *J. Thorac. Cardiovasc. Surg.* **109**, 885–891 (1995).

2. H. Li, W. Hsu, M. L. Lee, H. Wang, "A piecewise Gaussian model for profiling and differentiating retinal vessels," *Proc. Int. Conf. Image Proc.*, Vol. 1, 1069–1072 (2003).

3. H. Narasimha-Iyer, J. M. Beach, B. Khoobehi, B. Roysam, "Automatic identification of retinal arteries and veins from dual-wavelength images using structural and functional features," *IEEE Trans. Biomed. Eng.* **54**(8), 1427–1435 (2007).

4. A. M. Mendonça, A. Campilho, "Segmentation of retinal blood vessels by combining the detection of centerlines and morphological reconstruction," *IEEE Trans. Med. Imag.* **25**(9), 1200–1213 (2006).

5. Y. Wang, D. Hu, Y. Liu, M. Li, "Cerebral artery-vein separation using 0.1-Hz oscillation in dual-wavelength optical imaging," *IEEE Trans. Med. Imaging* **30**(12), 2030–2043 (2011).

6. X. Zhong, Y. Wang, M. Li, Y. Liu, "Separation of arteries and veins from optical imaging of intrinsic signals using independent component analysis," *ICICIP* **1**, 225–229 (2011).

7. D. Hu, Y. Wang, Y. Liu, M. Li, F. Liu, "Separation of arteries and veins in the cerebral cortex using physiological oscillations by optical imaging of intrinsic signal," *J. Biomed. Opt.* **15**(3), 036025–036025 (2010).

8. I. Vanzetta, R. Hildesheim, A. Grinvald, "Compartment-resolved imaging of activity-dependent dynamics of cortical blood volume and oximetry," *J. Neurosci.* **25**(9), 2233–2244 (2005).

9. J. D. Briers, Webster, "Laser speckle contrast analysis (LASCA): A nonscanning, full-field technique for monitoring capillary blood flow," *J. Biomed. Opt.* **1**(2), 174–179 (1996).

10. N. Prakash, F. Uhlemann, S. A. Sheth, S. Bookheimerf, N. Martinh, A. W. Togaa, "Current trends in intraoperative optical imaging for functional brain mapping and delineation of lesions of language cortex," *NeuroImage* **47**(2), T116–T126 (2009).

11. J. D. Briers, "Laser speckle techniques in biology and medicine," *Proc. SPIE* **2083**, 238–249 (1994).

12. D. A. Boasand, A. K. Dunn, "Laser speckle contrast imaging in biomedical optics," *J. Biomed. Opt.* **15**(1), 011109–011109 (2010).

13. R. Bonner, R. Nossal, "Model for laser Doppler measurements of blood flow in tissue," *Opt. Appl.* **20**(12), 2097–2107 (1981).

14. P. Miao, H. Lu, Q. Liu, Y. Li, S. Tong, "Laser speckle contrast imaging of cerebral blood flow in

freely moving animals," *J. Biomed. Opt.* **16**(9), 090502–090502 (2011).

15. A. Grinvald, E. Lieke, R. D. Frostig, C. D. Gilbert, T. N. Wiesel, "Functional architecture of cortex revealed by optical imaging of intrinsic signals," *Nature* **324**(6095), 361–364 (1986).

16. E. M. C. Hillman, "Optical brain imaging *in vivo*: Techniques and applications from animal to man," *J. Biomed. Opt.* **12**(5), 051402 (2007).

17. A. K. Dunn, A. Devor, H. Bolay, M. L. Andermann, M. A. Moskowitz, A. M. Dale, D. A. Boas, "Simultaneous imaging of total cerebral hemoglobin concentration, oxygenation, and blood flow during functional activation," *Opt. Lett.* **28**(1), 28–30 (2003).

18. http://omlc.ogi.edu/spectra/hemoglobin/.

19. Y. Wang, D. Hu, "Separation of cortical arteries and veins using intrinsic optical signals extracted by canonical correlation analysis," *ICDMA*, 1082–1085 (2011).

20. J. M. Geusebroek, A. W. M. Smeulders, J. Weijer, "Fast anisotropic Gauss filtering," *IEEE Trans. Imag. Process.* **12**(8), 938–943 (2003).

21. J. Lu, H. Lin, Z. Pan, "Adaptive region growing algorithm in medical images segmentation," *J. Comput.-Aided Des. Comput. Graph.* **17**(10), 2168–2173 (2005).

22. P. Miao, M. Li, H. Fontenelle, A. Bezerianos, Y. Qiu, S. Tong, "Imaging the cerebral blood flow with enhanced laser speckle contrast analysis (eLASCA) by monotonic point transformation," *IEEE Trans. Biomed. Eng.* **56**(4), 1127–1133 (2009).

23. M. Karaman, M. A. Kutay, G. Bozdagi, "An adaptive speckle suppression filter for medical ultrasonic imaging," *IEEE Trans. Med. Imaging* **14**(2), 283–292 (1995).

24. A. Mehnert, P. Jackway, "An improved seeded region growing algorithm," *Pattern Recogn. Lett.* **18**, 1065–1071 (1997).

25. B. Sahiner, N. Petrick, H. P. Chan, L. M. Hadjiiski, C. Paramagul, M. A. Helvie, M. N. Gurcan, "Computer-aided characterization of mammographic masses: Accuracy of mass segmentation and its effects on characterization," *IEEE Trans. Med. Imaging* **20**(12), 1275–1284 (2001).

26. J. M. Beach, K. J. Schwenzer, S. Srinivas, D. Kim, J. S. Tiedeman, "Oximetry of retinal vessels by dual-wavelength imaging: Calibration and influence of pigmentation," *J. Appl. Physiol.* **86**, 748–758 (1999).

27. P. S. Liao, T. S. Chen, P. C. Chung, "A fast algorithm for multilevel thresholding," *J. Inf. Sci. Eng.* **17**, 713–727 (2001).